Dosimetry data from fuel channel clips for benchmarking a new computational fluid dynamics model in neutron transport

Michael Manahan[1,*]

[1]MP Machinery and Testing (MPM), LLC, 2161 Sandy Drive, State College, PA 16803, USA

Abstract. Accurate neutron transport models for BWRs are needed to characterize neutron damage to the top guide, top guide cylinder, vessel nozzles, and to other upper internals. In the past, neutron transport calculations above top-of-active-fuel (TAF) have had large uncertainties (well in excess of ± 20%) mainly due to the fact that the steam density distribution in that region is not well known. An advanced three-dimensional (3D) neutron transport model, which incorporates computational fluid dynamics (CFD) in the code suite, has been developed. Retrospective dosimetry measurements were made to benchmark the transport results. Six fuel channel clips were removed from the top of the fuel bundles, and small disk-shaped dosimetry samples were cut from the clips. The cuts were made through the Inconel spring and through the stainless steel clip body. The clips were selected from bundles that cover regions of low, intermediate, and high steam density. The average C/M ratio for the 10 dosimeters is 1.06. It has been shown that all of the calculated dosimeter activities fall within ± 20% of the measurement. This meets the criterion set by RG 1.190 [1] for acceptability of the calculations.

1 Introduction

Previous neutron transport calculations above the top-of-active-fuel (TAF) in BWRs have had large uncertainties mainly due to the fact that the water density distribution in that region was not well known. Estimates of the uncertainties for fluences to the top guide and upper vessel regions are ~50% and higher. Previous neutron transport calculations have assumed a constant steam void fraction, typically ~80 % void fraction, in the region between TAF and the steam separator inlets. Although it was recognized that this is a coarse approximation, an accurate spatial distribution of the steam density was not available in the past. As a result of the approximation, the analytic uncertainty analysis of fluences to components located above the grid beam resulted in values far in excess of 20 percent. Regulatory Guide 1.190 targets uncertainties to be within 20% for the beltline region calculations, and it is reasonable to assume that this level of uncertainty can be achieved for fluences calculated outside of the active fuel region.

* Corresponding author: MPManahan@MPMachineryandTesting.com

2 Computational fluid dynamics (CFD) model

Fluid flow through a BWR presents a complex three-dimensional fluid dynamics problem due to the presence of multiple fluids interacting with each other. The fluid flow and mixing is governed by factors such as the physical properties of these fluids, flow velocities, geometry of the flow channel, and the interphase heat and mass transfer between fluids. The flow that leaves the core consists of steam and water, and these two components are partitioned as follows: steam flow from the bundles; subcooled water-rod flow; and subcooled bypass flow in-between the bundles. The water-rod flow mixes with the bundle steam near the top of the bundles below the upper tie plate (UTP). As this mixed fluid and the bypass water emerge from the bundles, they mix with each other in the space above the top guide (also referred to as the grid beam). This fluid mixing and flow evolution process dictates the properties of the composite fluid in the region between TAF and the steam separator dome.

2.1 CFD model description

The overall objective of the CFD modelling effort is the determination of the spatial distribution of the volume fraction of steam in the region above TAF. To accomplish this, a fluid volume mesh was created that extends from the grid beam top surface to the spherical dome-shaped surface at which the steam enters the stand-pipes in the steam separator dome. As with the TORT [2] neutron transport model, it is only necessary to create a quarter-core CFD model due to geometric symmetry. The 0° to 90° quadrant was modeled for the three plant (operating US BWR) cycles for which the dosimeters were analyzed. Figure 1 is a 3D view of the quarter-symmetric model showing the top guide cylinder, grid beam, steam separator, spargers, and fuel bundles in their respective positions. Outside of the shroud, the downcomer water is subcooled and is modeled as such.

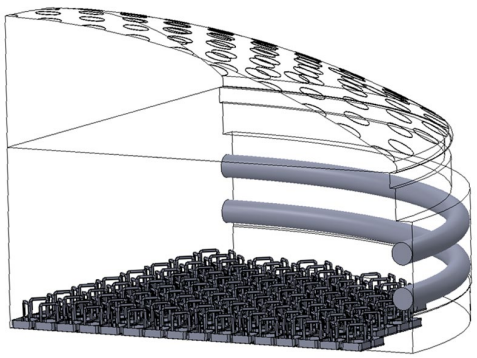

Fig. 1. 3D view of CFD model showing steam separator, top guide, grid beam, spargers, and fuel bundles.

The three fuel cycles analyzed as part of the benchmarking have two or more fuel types. In order to capture the physics for the three-dimensional flow accurately, the CFD geometry included models of all of the fuel types at their respective positions in the core. Further, each fuel bundle is accompanied by a bail-handle and an UTP which acts as a flow obstruction for the steam exiting the fuel bundle. Both the UTP and fuel rods were modelled so that the inlet boundary conditions provided by the SIMULATE-3 [3] output could be accurately represented.

2.2 CFD model output

An analysis was conducted to determine whether a cycle-by-cycle CFD analysis is needed in order to improve the neutron transport model above TAF to yield accurate calculated-to-measured (C/M) ratios. It was concluded that a cycle-by-cycle CFD analysis is needed. Not only are there large average density differences between cycles, but there are also large differences in the spatial distribution of steam for each cycle. The observed cycle differences are due mainly to differences in fuel design. An important fuel design difference is the size of the gap between bundles. This gap between bundles is related to the outer channel dimensions and the bundle corner geometries. A larger gap between bundles, and between bundles and the grid beam, allows for a larger flow area for the subcooled bypass water. This affects the spatial distribution in the mixing region above the grid beam. Also, flow areas for the bundles affect flow velocities. Therefore, bundle geometry plays an important role in the spatial distribution of the steam. The void fraction inlet conditions play a critical role in both the overall average fluid density and the fluid density distribution. Because void fraction has a direct effect on fluid density, the average void fraction of the bundles affects the overall fluid density. Further, the bundle locations affect the density distribution across the fluid volume. Bundle flow rates also have an effect on the steam density distribution.

An example water volume fraction distribution is shown in Figure 2 along with the radial and azimuthal distribution at an elevation of 50 cm above the grid beam. The previous assumption of an 80% void fluid inside the top guide and above the grid beam was found to be overly conservative by a significant amount over most of the steam dome region. The average bundle exit void fraction across the bundles for each cycle analyzed ranged from 74.2% to 80.5%, making 80% void seem like a good assumption. However, the CFD simulations show that while the void fraction for the steam above the grid beam is less than 80% over the central core region, much higher density water is observed near the periphery which causes large reductions in neutron flux at the top guide and upper vessel region. The lower density fluid in the central core region reduces the likelihood of neutron scattering toward the top guide, but this effect is small compared to the reduction associated with high density steam at the periphery.

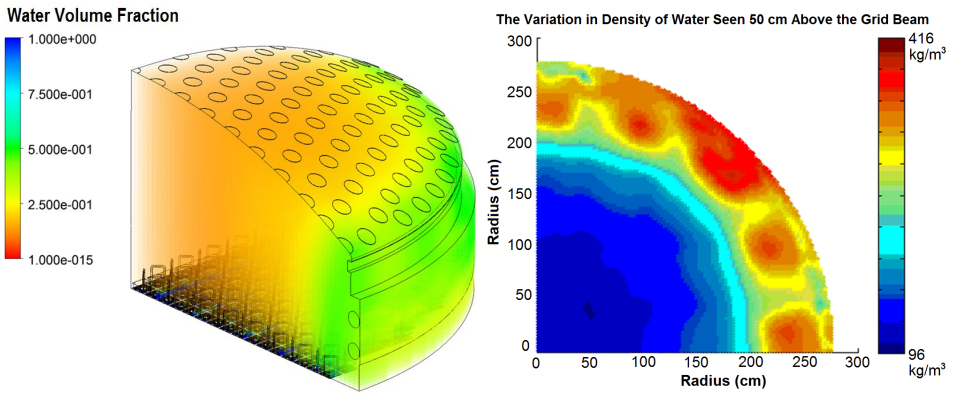

Fig. 2. (Left) Example of CFD determined water volume fraction distribution. High density steam is observed between the top guide and the outer fuel bundles. (Right) Plot showing the radial and azimuthal variation of water density at an elevation 50 cm above the grid beam.

2.3 Effect of water density distribution on neutron transport

As discussed, the steam density in the central portion of the top guide volume is lower than previously assumed in neutron transport models, and the density at the periphery near the top guide cylinder inner diameter surface is much higher. TORT analyses were conducted to quantify the impact of the CFD results. A large reduction in the flux is observed for upper region top guide cylinder welds and also for the pressure vessel. An example of the flux reduction to top guide cylinder vertical welds V5 and V6 is shown in Figure 3. The reduction in flux is a result of high density steam which is observed in the CFD output between the top guide and the outer fuel bundles (Figure 2). This steam acts as a very effective shield for the top guide cylinder and upper vessel, reducing the flux to approximately 1/6th of the previous 80% void case transport fluxes.

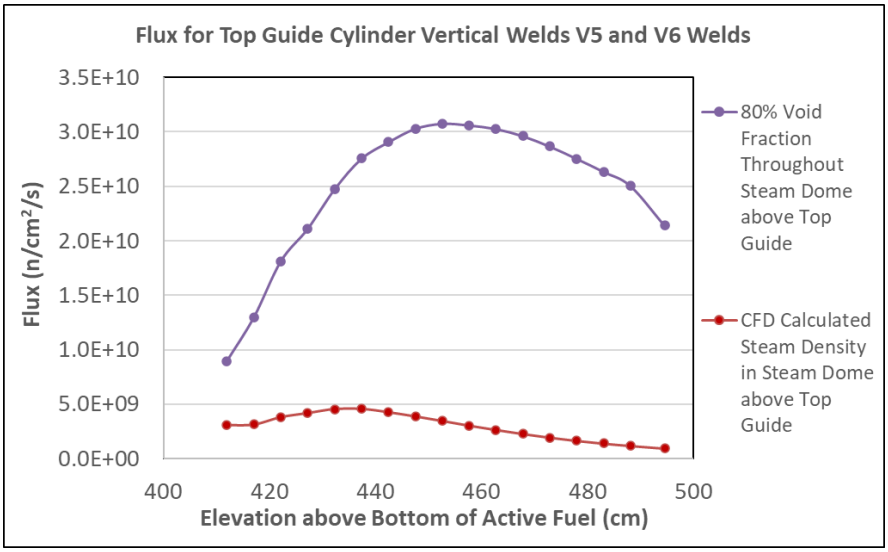

Fig. 3. Comparison of top guide vertical weld fast (E>1 MeV) fluxes determined using the CFD calculated water density compared to the fast flux determined assuming 80 % void fraction above the grid beam.

Similarly, Figure 4 shows the peak vessel fast (E>1 MeV) fluence at 54 EFPY calculated using both the CFD water density distribution and the 80% void fraction assumption. Of particular interest is the non-physical peak shown in Figure 4 that occurs above the grid beam elevation (>400 cm elevation) in the 80% void model. This erroneous peak is due to the direct shine from the top of the core in the 80% void assumption case. The peak is not physically correct because the high density water between the core edge and the top guide cylinder provides very effective shielding which suppresses this local peak and keeps the fluences below 1.0 E17 n/cm^2 in this region of the vessel. If the peak were real, it may have caused several issues for the plant since it would require the inclusion of neutron damage effects for the upper shell course materials in the PT curves. In such a case, the upper shell course materials would need to be considered in the plant pressure vessel surveillance program.

3 CFD benchmark results

Conventional dosimetry was not available for benchmarking the CFD model. Therefore, a decision was made to cut material from fuel channel fasteners for this purpose. Six fuel

channel fasteners (referred to as fuel clips) were removed from bundles which were irradiated in cycles leading up to the clip removal (cycles 19, 20, and 21). Two of the clips were irradiated in all three cycle (GEQ771/GEQ846), two were in C20 and C21 (GER212/GER238), and two were in C21 only (GES366/GES547). Other than one bundle (GER212), all of the bundles used for dosimetry were shuffled to a new location each cycle. As a result, the clips were exposed to widely varying water densities, thereby providing a very good benchmarking opportunity. Analysis of clip GER212, that was introduced in C20, was not done because the adjacent control rod was inserted about 60% of the way through C21 due to a failed fuel issue.

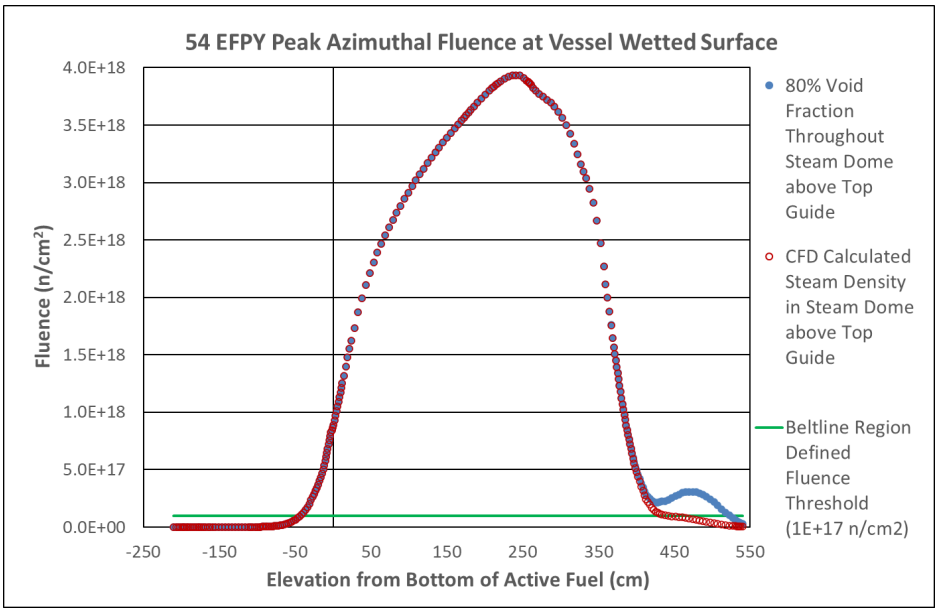

Fig. 4. Peak vessel fast (E>1 MeV) fluence at 54 EFPY. Transport results using CFD calculated water density are compared with the results assuming 80 % void fraction above the grid beam.

After the conclusion of cycle 21, the 6 clips were removed from the bundles and stored in a holder in the spent fuel pool. As a result of the high dose rates, MPM designed and built special cutting equipment to extract small disks from the clips for the specific activity measurements. A fuel channel clip after cutting is shown in Figure 5. The clips consist of an outer Inconel spring which is attached to the stainless steel body via a captive screw. Since the cuts were made through both the spring and fastener body, two dosimeter disks were obtained from each clip.

The primary focus of the CFD benchmark analysis is on the Fe54(n,p)Mn54 reaction. The short half-life of 70.82 days for the Ni58(n,p)Co58 reaction precluded obtaining accurate counting results. The only other reaction that could be considered is the Nb-93(n,n')Nb-93m reaction, but the high activity of the dosimetry materials precluded accurate counting for this reaction.

Fig. 5. Fuel channel fastener showing example of cut made to extract the retrospective dosimetry disks for specific activity measurements.

As mentioned, the TORT transport models with the CFD water density inputs were run for cycles C19 through C21, and a through-cycle analysis was included in the C21 calculations. The calculated fluences were determined at the center of the cut location for each clip. The accumulated fluence calculations included the fact that two of the bundles were moved to different locations at the end of C19 and C20, and two other bundles were moved at the end of C20. The calculation accounted for the increase in the channel length from 32.84 cm to 33.60 cm during operation due to channel swelling. The swelling model correlates channel length increase as a function of exposure. So, the channel growth axial span indicated in Figure 6 is largest for the bundles that were in for 3 cycles, and the lower limit is for the bundles that were introduced in C21. As shown in the figure, the clip sampling location is just above the top surface of the grid beam where the channel exit steam mixes with the subcooled bypass water. This is a challenging elevation for fluence determination as the water density in localized regions varies from 80 to 720 kg/m^3 across the core.

The Inconel and SS disks were lightly abraded and cleaned to remove oxide from the samples prior to counting and weighing. Radiometric analysis was performed using high resolution gamma emission spectroscopy. The total mass of each disk was measured using a high precision analytical digital balance. In retrospective dosimetry applications, it is necessary to measure the composition of the alloy. X-ray fluorescence measurements were made to determine the iron weight percent for each of the 10 disks. All iron mass measurements were made after irradiation.

The CFD model benchmark results are summarized in Table 1. The average C/M ratio for the 10 dosimeters is 1.06. For each dosimetry result, it has been shown that all of the calculated dosimeter activities fall within ± 20% of the measurement. This meets the criterion set by RG 1.190 for acceptability of the calculations.

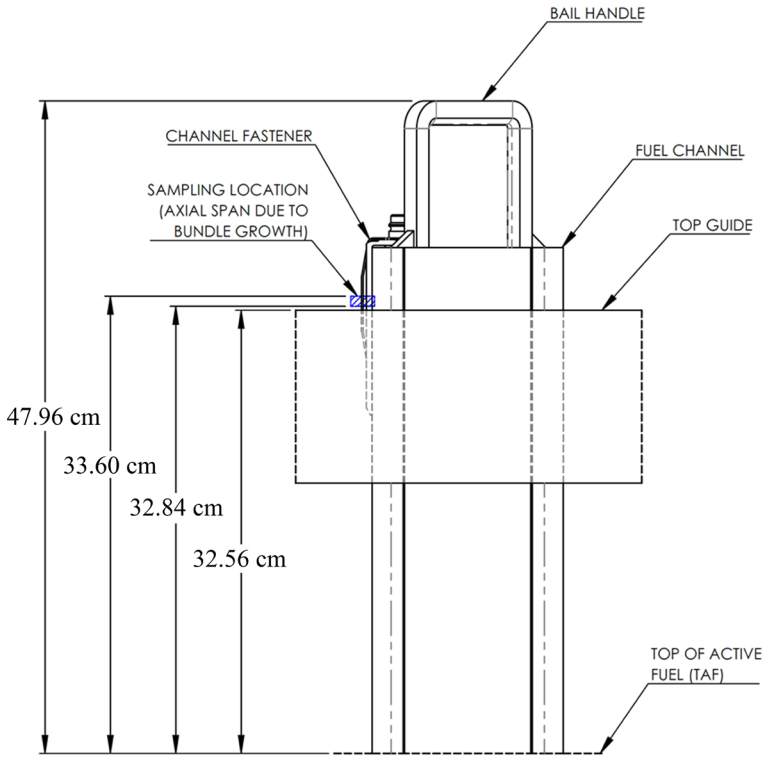

Fig. 6. Schematic representation of the channel fastener showing the locations where the fluence was calculated. The calculation accounted for channel length increase due to swelling.

As previously mentioned, two of the clips were irradiated in all three cycles (GEQ771/GEQ846), two were in C20 and C21 (GER212/GER238), and two were in C21 only (GES366/GES547). For BWRs, the average fuel cycle is 24 months. Other than bundle GER212, all of the bundle clips used for dosimetry were shuffled to a new location each cycle. As a result, the clips were exposed to widely varying water densities, thereby providing a very good CFD model benchmarking opportunity. Accounting for the Mn54 half-life of ~300 days, the C21 activation will be a good record of steam distribution effects on the flux history. However, more than 80% of the activity from the previous cycle will have decayed. The power history was weighted to account for the time varying effects on the dosimetry. The benchmarking is properly viewed as a one cycle benchmark with varying water density at each of the clips. In particular, during C21, two clips were located near core center, two were located at a position of 3 to 4 bundles in from the periphery, and two were located at the periphery.

Table 1. CFD model dosimetry benchmark results.

Dosimeter Reaction	Measured (M) Activity (dps/mg)	Calculated (C) Activity (dps/mg)	Ratio (C/M)
Fasteners Introduced in C21			
GES366S Fe54(n,p)Mn54	34,042.1	37,179.4	1.092
GES366I Fe54(n,p)Mn54	31,673.2	37,179.4	1.174
GES547S Fe54(n,p)Mn54	24,667.3	24,451.6	0.991
GES547I Fe54(n,p)Mn54	23,373.2	24,451.6	1.046
Fasteners Introduced in C20			
GER238S Fe54(n,p)Mn54	41,395.0	42,581.8	1.029
GER238I Fe54(n,p)Mn54	36,850.8	42,581.8	1.156
Fasteners Introduced in C19			
GEQ771S Fe54(n,p)Mn54	13,674.0	12,858.7	0.940
GEQ771I Fe54(n,p)Mn54	11,929.1	12,858.7	1.078
GEQ846S Fe54(n,p)Mn54	22,857.3	23,005.3	1.006
GEQ846I Fe54(n,p)Mn54	20,802.4	23,005.3	1.106
		Average Iron Result	1.062

4 Uncertainty analysis for above core structures

The fluence uncertainty at upper internals and vessel nozzles above TAF has contributions in addition to those typically considered in the core region. These added uncertainty contributors are:

- Additional transport methodology uncertainty in upper and lower regions
- Above core steam density uncertainty
- Additional steel transport uncertainty
- Additional core top and bottom edge power uncertainty
- Weld and nozzle location uncertainty

The above core steam density uncertainty estimates in Table 2 were derived from data generated from CFD parametric studies. The deterministic model improvements, such as buoyancy and compressibility, are not included in Table 2 because there are no uncertain inputs involved.

Combining all of the uncertainties in the active fuel region, as well as those above TAF, yields the following results:

- Horizontal/vertical shroud weld fluence uncertainties range from 13.3% to 19.0%
- Vessel plates, welds, and nozzles above TAF range from 17.4% to 19.4%.

5 Conclusions

The uncertainty analysis demonstrates that the MPM calculational methods provide fluence results within allowable tolerance bounds (±20%) for the reactor vessel, shroud welds, and

surveillance capsules which lie within the axial active fuel region. This satisfies the requirements of RG 1.190. However, RG 1.190 does not address uncertainty and benchmarking outside this region. Nevertheless, analytic uncertainty evaluations of structures outside the beltline region have been made, and, especially above the core, uncertainties are within the RG 1.190 desired ± 20%. This low uncertainty level was only achievable by inclusion of the CFD model within the transport code suite. Retrospective dosimeters were cut from fuel channel clips and these data were used to benchmark the use of CFD data in the transport model. The average C/M ratio for the 10 dosimeters is 1.06. For each dosimetry result, it has been shown that all of the calculated dosimeter activities fall within ± 20% of the measurement. This meets the criterion set by RG 1.190 for acceptability of the calculations in the active fuel region.

Table 2. CFD water density overall uncertainty.

Uncertainty Contributor	Units	Best Case Input Used	Perturbed Input	Average Percent Difference (%)	σ Level	1σ Uncertainty (%)
Downcomer Water Temperature for Heat Transfer Through the Top Guide Wall	°C	275.1	287.8	5.73	3	1.91
Water/Steam Heat Transfer Coefficient	W/(m^2°C)	3123	4259	5.04	3	1.68
Water Droplet Size	Microns	1.0	2.3	6.36	3	2.12
Drag Coefficient	None	0.44	2.732	0.65	1	0.65
Mesh Refinement (Maximum Element Size in Mesh)	mm	60.76	30.87	1.90	1	1.90
Convergence	Iterations	100	400	1.80	3	0.60
TOTAL						3.92

References

1. US NRC Regulatory Guide 1.190, 'Calculational and Dosimetry Methods for Determining Pressure Vessel Neutron Fluence' , USNRC, Rockville, MD, (2001).
2. RSICC Computer Code Collection, CCC-543, TORTDORT-PC, Two- and Three-dimensional Discrete Ordinates Transport Version 2.7.3, Available from the Radiation Safety Information Computational Center, Oak Ridge National Laboratory, Oak Ridge, TN, (1996).
3. CASMO/SIMULATE, Studsvik's Advanced Three Dimensional Two-Group Reactor Analysis Code, Studsvik of America, Inc. (2020)